

## Letter

## Optical and electrical multilevel storage in organic memory passive matrix arrays



Peter O. Körner, R. Clayton Shallcross, Eduard Maibach, Anne Köhnen, Klaus Meerholz\*

University of Cologne, Department of Chemistry, 50939 Cologne, Germany

## ARTICLE INFO

## Article history:

Received 17 July 2014

Received in revised form 4 October 2014

Accepted 12 October 2014

Available online 27 October 2014

## Keywords:

Multilevel memory

Photochromic

Organic diode

Passive matrix array

Crosstalk

## ABSTRACT

The integration of organic memory diodes, based on photochromic transduction layers, into a simple cross-bar passive matrix array is presented. We show that the high rectification ratios of these diodes successfully suppresses crosstalk effects in these devices, thus avoiding the necessity to integrate additional diodes or transistors. We compare the passive matrix devices' performance to that of non-crossbar reference devices and discuss their performance limitations related to edge effects, which are a consequence of the fabrication process. Finally, we show that the analogue response of the current density to incremental switching of the transduction layer can be used for multi-level programming of the memory elements with no inherent limit to the number of intermediate states. We demonstrate the successful read-out of 8 current levels in a prototype device via both optical and electrical writing procedures.

© 2014 Elsevier B.V. All rights reserved.

## 1. Introduction

Organic electronic devices have attracted wide interest due to their potential for simple and inexpensive fabrication over large areas and on flexible substrates. Such processing benefits are enabled by the solubility of organic materials in various solvents (i.e., the ability to process device active layers from solution precursors that permit the utilization of high-throughput, low-temperature and inexpensive printing techniques for structured device fabrication). For many of the envisioned applications of organic electronics (e.g., RFID tags), non-volatile organic memory technologies are essential. The vast majority of organic memory proposed in the literature are binary memory devices, which can be programmed to either one of two distinguishable states (i.e., “1” or “0”) [1–4]. However, multi-level systems can potentially lead to an increased data storage density without the necessity of

reducing the size of a singular memory element (e.g., NAND flash memory stores 4 bits per cell [5]). Few examples of such multi-level organic memories can be found in the literature and their working mechanisms are usually only demonstrated on one singular memory element [6–12]. However, in order for such systems to be employed as actual memory technologies the statistically viable number of addressable levels needs to be tested in an array of memory elements.

The simplest layout for an integrated collection of memory devices is a passive matrix array in which the active materials are sandwiched between two electrodes in a cross-bar geometry [13,14]. Such passive memory arrays feature the maximum density of memory elements as each cell occupies an area of only  $4f^2$ , where  $f$  is the feature size (meaning the electrodes' width as well as spacing between cells). Fabrication of such passive memory arrays is simple and inexpensive, but they may suffer from crosstalk between different memory elements (illustrated in the SI Fig. S1), leading to unreliable read-out of the stored information [15]. The cross-talk problem can be avoided

\* Corresponding author.

E-mail address: [Klaus.Meerholz@uni-koeln.de](mailto:Klaus.Meerholz@uni-koeln.de) (K. Meerholz).

by integrating rectifying diodes or transistors, which are electrically connected in series with the resistive memory elements [16,17]. Alternatively, the memory element itself could be rectifying [4,13,14], but most examples of multi-level elements found in the literature are not.

We have recently reported on solution-processed non-volatile organic memory devices fabricated by integrating a cross-linkable dithienylethene (XDTE, SI Fig. S2a) as a transduction layer into the layer stack of organic light-emitting diodes [18,19]. The photochromic XDTE molecules can be reversibly switched between two energetically distinct and thermally stable isomers, and their difference in HOMO energy can be exploited as a switchable hole-injection barrier in organic diodes and thus control the current flowing through such a device. While the optical switching of DTEs has been extensively studied [20–22], recent studies have shown that the ring-closing reaction can also be induced electrochemically and electrically [23,24]. We have recently investigated how these solid-state switching phenomena can be used to optically and electrically program XDTE-based organic memory diodes into a continuum of intermediate states [25], providing a working methodology for the multilevel passive memory arrays presented here. Due to the mechanism of electrical switching, the accessible dynamic range for intermediate states is about two orders of magnitude smaller than for optical switching. Furthermore, electrically induced switching of the molecules can only be reversed with optical irradiation; therefore, electrically, the XDTE-based organic memory diode behaves as “write once read many” (WORM) memory similar to EPROMs (Electrically Programmable Read Only Memory). More details about the operating principle of the organic memory devices are explained in the [Supporting Information](#) (Figs. S2 and S3).

In this paper, inspired by the high rectification that was observed for these devices ( $>10^4$ ), we report on the integration of these organic memory elements into a passive matrix array prototype and demonstrate multilevel capability for both, optical and electrical recording.

## 2. Experimental

Organic memory arrays are fabricated on pre-structured indium tin oxide (ITO,  $15 \text{ Ohms cm}^{-2}$ ) substrates purchased from Precision Optics Gera, Gera, Germany. The ITO is structured into finger electrodes by combined photolithography and wet chemical etching processes. For the  $3 \times 3$  matrices discussed in Section 3.1 the electrodes have a width of 2.8 mm and a spacing of 1.6 mm. The  $4 \times 4$  matrices discussed in Section 3.2 have electrodes of widths: 1.0 mm, 0.5 mm, 0.25 mm, and 0.1 mm. For the  $12 \times 12$  matrices discussed in Sections 3.3 and 3.4 the electrodes have a width and spacing of 0.5 mm, respectively.

Prior to their use the substrates are solvent cleaned and then UV-ozone treated for 15 min. PEDOT:PSS (Clevios P AI4083, 50 nm) is spin-coated in air and dried for 10 min at  $150^\circ\text{C}$ . The substrates are then transferred into a  $\text{N}_2$  glove box where the hole-transport materials (HTM1 and HTM2; oxetane-functionalized triphenylaminodimer

derivatives, see [25]) are spin coated from toluene solutions ( $5.0 \text{ mg mL}^{-1}$ , 15 nm) containing 2 mol% 4-octyloxydiphenyliodonium hexafluoroantimonate (OPPI) as crosslinking photoinitiator. After each spin-coating step, the film is irradiated with UV light (365 nm for 15 s), thermally cured ( $110^\circ\text{C}$  for 60 s) and rinsed with THF. The active switching layer of XDTE ( $9 \text{ mg mL}^{-1}$ , 6 mol% OPPI, 40 nm) in the photo-stationary state (PSS) is subsequently spin-coated from toluene, irradiated with UV light (312 nm for 60 s), thermally cured ( $110^\circ\text{C}$  for 3 min.) and rinsed with THF. Finally, the electron-transport material (ETM; commercially available blue-emitting polyspirobifluorene polymer, Merck KGaA) is spin-coated from toluene solution ( $10 \text{ mg mL}^{-1}$ , 70 nm). The molecular structures of HTM1, HTM2 and ETM have been previously reported [25]. Layer thicknesses are determined via surface profilometry with a Dektak 3. The cathode (4 nm Ba, 150 nm Ag) is evaporated through a shadow mask (with the exact same pattern as the ITO electrode) at a pressure of  $\leq 2.0 \times 10^{-6}$  mbar, affording top finger electrodes orthogonal to the ITO stripes. The samples are encapsulated (Araldite + 2000) for testing outside the glove box.

Current density–voltage (JV) measurements of the passive memory array prototypes are performed sequentially for all individual cells using a Keithley 2400 source meter and data is collected with a home-built LabView program. Optical programming of the devices is done with a laboratory UV lamp (312 nm, ring-closing) at an irradiation intensity of  $0.52 \text{ mW cm}^{-2}$ . Electrical programming is done via the application of varying numbers of 200 ms long pulses of a constant writing current density  $J_{\text{WRITE}} = 20 \text{ mA cm}^{-2}$ . Electrical read-out is carried out by measuring the current density ( $J_{\text{READ}}$ ) using 200 ms long pulses of 10 V (where the ON/OFF ratio is maximized). These  $J_{\text{READ}}$  values are then normalized to the current densities measured in the all ON state to eliminate process-related systematic variations (see SI for details). Optical erasure is done with an orange LED (600 nm, 2.3 V, 600 mA, ring-opening).

## 3. Results and discussion

### 3.1. Cross-talk

First, we investigate whether the intrinsic rectifying behavior of the organic memory diodes can successfully suppress cross-talk effects in our passive matrix arrays. Initial cross-talk studies are tested for devices with a  $3 \times 3$  matrix layout, in which each of the nine individual cells has the same area ( $0.08 \text{ cm}^2$ ) as the previously reported “unstructured” devices [25]; however, we note that the passive memory array devices discussed here are quadratic in shape instead of circular (see Fig. S4). The JV-characteristics in forward and reverse bias in the ON as well as in the OFF state are shown for all nine cells in Fig. 1a (circles), compared with the data for a single pixel unstructured device (stars). In the ON state, above the turn-on voltage, the JV-curves of the passive matrix (PM) cells are essentially identical to those found for unstructured reference devices; however, the reverse current-density as well as the forward bias leakage current-density (in the range

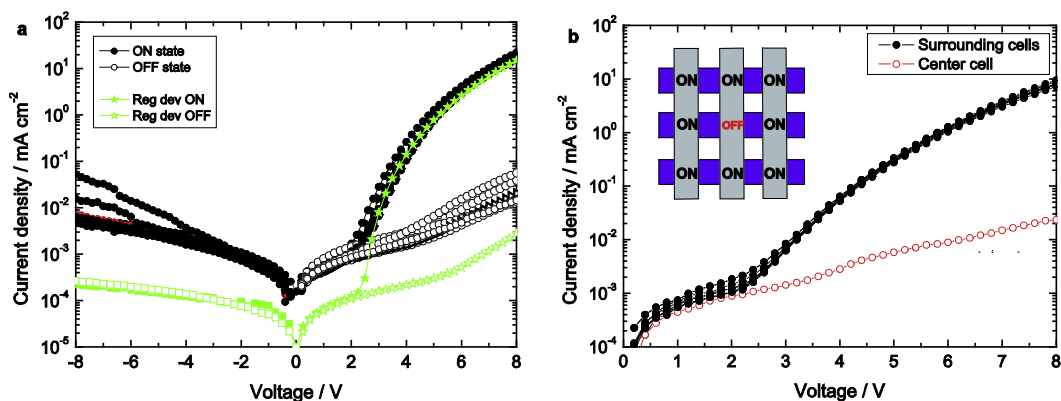


**Fig. 1.** Cross-talk in passive matrix arrays of organic memory diodes. (a) JV-characteristics of organic memory devices in a  $3 \times 3$  passive matrix (black symbols) in the all-ON (solid) or the all-OFF (open) state as well as of the “unstructured” reference devices ([25], green stars). Both devices feature the same device area of  $0.08 \text{ cm}^2$ . (b) JV-characteristics of the  $3 \times 3$  passive matrix with the center cell in the OFF state while the surrounding cells are in the ON state. (For interpretation of the references to colour in this figure legend, the reader is referred to the web version of this article.)

0–2 V) and hence the entire OFF state current-density are about one order of magnitude larger. As a result of the increased OFF current density the ON/OFF ratios of the PM cells are roughly one order of magnitude smaller ( $\text{ON/OFF ratio}_{\text{max}} \approx 10^3$  compared to  $10^4$  in the reference). The increased leakage currents in the PM cells are caused by edge effects occurring at the device perimeter, which will be discussed in detail in the next section. Apart from the reduced overall performance of the PM cells it should be noted that the cell-to-cell variation of the ON state current density is very small. By contrast, variation of the OFF state current density is naturally larger due to variations of the ITO edges.

To test for cross-talk the device is then put in the most challenging configuration in which the center cell is in the OFF state while the surrounding eight cells are in the ON state (see inset in Fig. 1b). This cross-talk testing configuration is accomplished by exposing the entire 9-element array in the OFF state to UV-illumination through a shadow mask where the center cell is blocked from the UV light and thus remains in the OFF state. The subsequently measured JV-characteristics of all nine cells are shown in Fig. 1b. Clearly the center cell can be read as OFF, with the same ON/OFF ratio as in the all-ON and all-OFF measurements (Fig. 1a). This result demonstrates that the rectifying behavior of the organic memory diodes allows passive matrix integration without the need for additional electrical circuit elements.

### 3.2. Leakage currents

As seen above the PM cells exhibit significantly larger leakage currents than the unstructured devices, providing a reduced ON/OFF ratio for PM cells. One may assume that the increased leakage current measured when an individual cell is addressed is in fact the parasitic leakage current of the entire array, which would be higher than the real leakage current of the individual cell, because the finite rectification ratio of the diodes will always allow a certain amount of cross-talk. In order to test the effect of cross-talk

on leakage current in a passive memory array, Fig. S5 shows the JV-characteristics of 12 organic memory devices ( $0.0025 \text{ cm}^2$ ) that are fabricated in a cross-bar geometry; however, only a single finger electrode is evaporated as top contact, on a substrate comprised of 12 individual ITO anodes (see inset in Fig. S5). Consequently this device is not a passive matrix array and cross-talk effects are not possible. Nevertheless, the leakage current density of these devices is even worse, about two orders of magnitude larger than that of the non-crossbar devices (stars). In this case, the issue related to elevated OFF (leakage) currents is exacerbated relative to the aforementioned  $3 \times 3$  passive matrix array ( $0.08 \text{ cm}^2$ ), because this  $1 \times 12$  layout provides cells with a smaller device area ( $0.0025 \text{ cm}^2$ ). This data leads to the conclusion that the elevated leakage currents, which are responsible for the diminished ON/OFF ratio of these passive memory arrays originate from the cross-bar geometry itself.

The polyspirobifluorene polymer used as ETM in the organic memory layer stack is a blue emitter, therefore the device is also an OLED. The device emission exhibits ON/OFF ratios of the same order of magnitude as the current density. While the luminescence can thus, in principal, be used as alternative read-out channel [18], it provides a convenient means to visualize the leakage currents in the PM cells. Fig. 2a shows a photographic image of one of the PM cells in the OFF state. It can be seen that while the majority of the active device area shows essentially no emission, there is considerable emission coming from the ITO anode edges of the device. This observation implies that in the OFF state the majority of the current is flowing through the edges of the device.

To find the origin behind these effects, we prepared a cross-section of the passive memory array and imaged the edge of the ITO anode using scanning electron microscopy (SEM; Fig. 2b). Obviously the combined thickness of all organic layers is significantly smaller at the edge of the ITO anode (100 nm) than at the device center (210 nm). This thinning is a result of the spin-coating process and ultimately leads to a reduction of the ON/OFF ratio

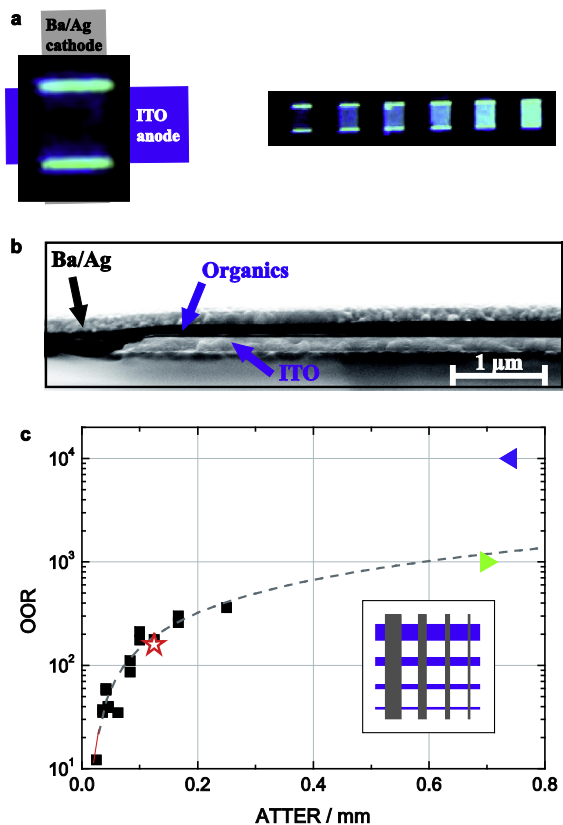


**Fig. 2.** Leakage currents through the edges of organic memory devices in cross-bar geometry. (a) Left: Photograph of a crossbar organic memory cell in the OFF state at 10 V (area  $0.0025 \text{ cm}^2$ ). For clarity the orientation of the electrodes is schematically displayed. Right: Photograph of six cells in different memory states. (b) Cross-section image obtained by SEM. (c) ON/OFF-ratio of organic memory devices in cross-bar geometry shown in the inset (squares) plotted as a function of the respective area to total edge ratio (ATTER). The dashed line is a linear fit (note the log–lin scale) to the data. The data point of the above discussed  $3 \times 3$  device is shown as right-handed green triangle, the data point for the  $1 \times 12$  device is shown as red star and the data for an unstructured device is shown as left-handed blue triangle. (For interpretation of the references to colour in this figure legend, the reader is referred to the web version of this article.)

of our organic memory devices. We note that there is a strong dependence of the ON/OFF ratio on the XDTE layer thickness (see Fig. S6), which is a compromise between two counteracting effects: on the one hand, thicker layers will limit the ON current, due to the low mobility of XDTE; on the other hand, thinner layers will not properly block holes. The maximum ON/OFF ratio is significantly smaller for thinner layers and is also shifted to lower voltages. At the readout voltage of 10 V for the passive memory array devices, the ON/OFF ratio for these thinned XDTE layers at the device edges may be close to unity. This is in agreement with our observation that the light intensity at the edges does not seem to vary much for organic memory cells in different memory states (Fig. 2a).

To further investigate how the ratio of the device edge and the active area relates to the leakage current we fabricated PM cells of varying sizes in a  $4 \times 4$  layout on a single substrate (see Section 2 and inset of Fig. 2c). The resulting

16 crossbar devices exhibit different active areas, and, more importantly, different ratios of device area to device edge length. Fig. 2c shows the ON/OFF ratio as a function of the area to total edge ratio (ATTER). There is a linear relationship between ON/OFF ratio and ATTER, confirming that the ON/OFF ratio is indeed limited by device edge leakage currents of each individual cell rather than cross-talk effects in the passive matrix array. Please note, that the data obtained using the other crossbar geometries ( $3 \times 3$ ,  $1 \times 12$ , and  $12 \times 12$ , as discussed above and below) fall onto this line, while the non-crossbar reference does not. The reason for the superior performance of the latter is that these have been fabricated on unstructured ITO substrates (compare experimental section in [25] and Fig. S3) on which the spin-coating process generally produces homogeneous films.

### 3.3. Optical multi-level programming

We next investigate multi-level programming in  $12 \times 12$  passive memory arrays prototypes. In this layout, defects caused by fabrication imperfections could not be completely avoided, since we are currently unable to fabricate the devices in a clean room. Fig. 3 shows the JV-characteristics of a passive memory array prototype with 120 functional memory cells for the ON state (black) and the OFF state (grey) as well as the calculated ON/OFF ratio (red). All cells exhibit an ON/OFF ratio larger than  $10^2$  at 10 V. The cell-to-cell variation is small and mainly observed in the OFF state, as expected (see above).

Next, we create a response curve for optical programming (Fig. 4a). Starting with all cells in the OFF state, we illuminate the device with UV light through a slit-shaped shadow mask (1 mm width), so that a line of 12 individual cells featuring a common cathode were irradiated by different UV-doses at the same time. The  $J_{\text{READ}}$  values in Fig. 4a are an average of the current density values at 10 V (i.e., where the ON/OFF ratio is maximized for this device) for cells illuminated with a specified UV dose. There is a steep increase in  $J_{\text{READ}}$  up to exposure doses of ca.  $150 \text{ mJ/cm}^2$ , followed by a much slower increase. We

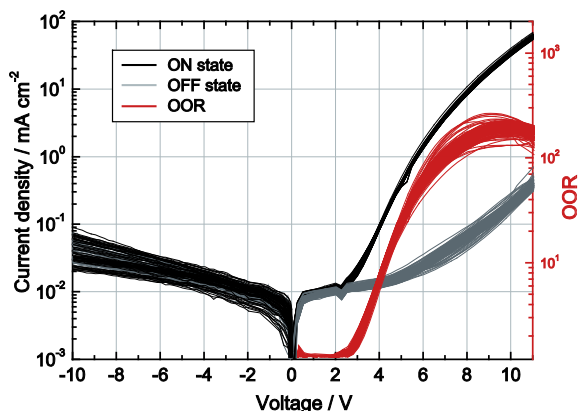


**Fig. 3.**  $12 \times 12$  passive memory array for multi-level programming. JV-characteristics of a 120-pixel organic memory passive matrix array ( $0.0025 \text{ cm}^2$  cell area).

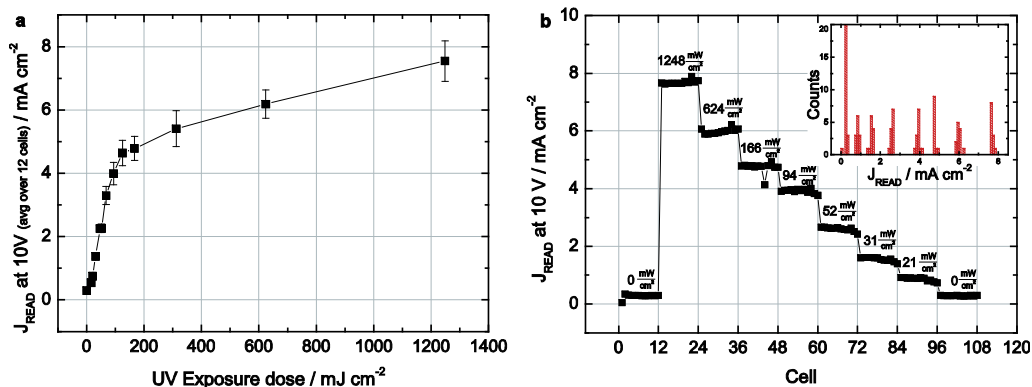


**Fig. 4.** Optical multi-level programming. (a) Optical response curve:  $J_{\text{READ}}$  as a function of UV exposure dose. The displayed values have been averaged over 12 devices. The line is a guide to the eye. (b) Readout of the optically programmed passive memory array. Inset: corresponding histogram.

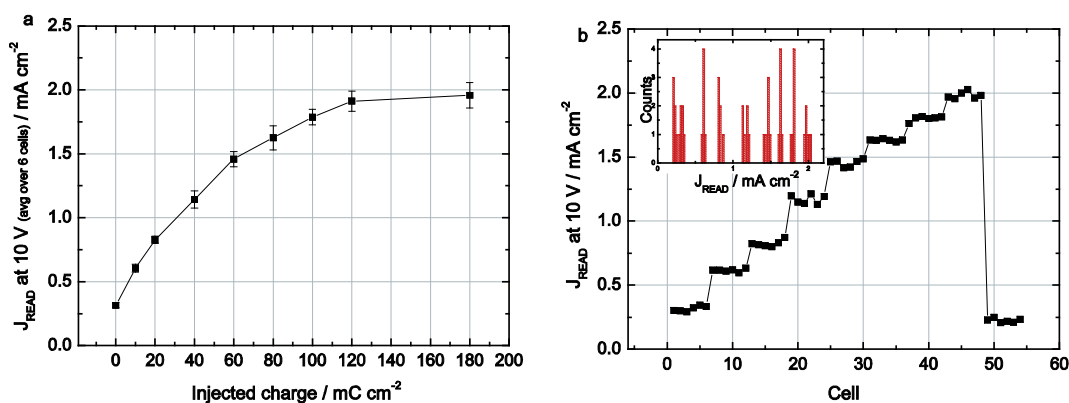


**Fig. 5.** Electrical multi-level programming. (a) Electrical response curve:  $J_{\text{READ}}$  as a function of the injected charge ( $Q_{\text{inj}}$ ). (b) Readout of the electrically programmed passive memory array. Inset: Corresponding histogram.

did not observe a leveling to the photo-stationary state (PSS), which is expected after infinitely long expose. Practically, only the initial (ideally) linear response range is useful considering the intensity used here ( $0.52 \text{ mW cm}^{-2}$ ), which corresponds to recording times of up to 5 min. Please note, however, that there is a linear relationship between intensity and switching speed (see the SI in our previous work [25]), implying that sub-second writing times can be expected for high intensity sources (e.g.,  $1 \text{ W cm}^{-2}$ ).

Based on the optical response curve, we optically program eight roughly equidistant states into our passive memory array prototype. The normalized  $J_{\text{READ}}$  values (see Experimental section and Fig. S7 for normalization details) are shown in Fig. 4b. It is clear from the lack of overlap of the histogram data that the eight levels can be written and retrieved without error.

### 3.4. Electrical multi-level programming

By passing defined amounts of charge through individual cells, we are able to electrically program our XDTE organic memory passive memory arrays. Please note, that this electrical recording is achieved at current densities

at least two orders of magnitude higher than  $J_{\text{READ}}$  ( $V_{\text{WRITE}} = 15\text{--}20 \text{ V}$ ;  $V_{\text{READ}} = 10 \text{ V}$ ). Therefore, readout is non-destructive (see Fig. S8).

We create a response curve equivalent to that seen for optical programming by averaging the measured  $J_{\text{READ}}$  over 6 individual cells (Fig. 5a). Charge injection beyond  $Q_{\text{inj}} = 120 \text{ mC cm}^{-2}$  has no additional effect on  $J_{\text{READ}}$ , implying that the electrical closing reaction is saturated. For a write current density of  $20 \text{ mA cm}^{-2}$ , an injected charge density of  $120 \text{ mC cm}^{-2}$  corresponds to recording times of up to 6 s. Please note, that the dynamic range for electrical programming is smaller by roughly a factor of 4, because it is inherently self-limiting, due to the formation of preferred conduction pathways (filaments), which we have discussed in detail in our previous work [25].

If the writing current flows predominantly through the device edges for passive memory arrays, one might suspect that the problem of edge leakage current might limit the electrical switching effect altogether. By contrast, Fig. 2a shows that electrical programming of a cell occurs across the whole device, despite the edge leakage effect.

Following the procedure already described above for optical recording, we demonstrate electrical programming of eight roughly equidistant states into our passive

memory array prototype. As evidenced by the lack of overlap between the current levels presented in the histogram plot, Fig. 5b shows that all levels could be retrieved without error. These results demonstrate that the electrical programming procedure does not lead to undesired switching in neighboring cells due to cross-talk effects.

#### 4. Conclusion

We have demonstrated that solution-processed, multi-layer, organic memory diodes based on photochromic crosslinkable dithienylethenes can be integrated into passive-matrix arrays since their rectifying behavior effectively suppresses cross-talk. At this point, the performance of our organic memory passive memory arrays, in terms of ON/OFF ratio, is reduced compared to their previously reported unstructured counterparts, due to device edge leakage currents. Nonetheless the possibility of optical and/or electrical multi-level programming is successfully demonstrated in these prototypes; however, we note that, since the electrically written levels must be erased optically, all electrical programming corresponds to write-once-read-many (WORM) memory similar to EPROMs (Electrically Programmable Read Only Memory). We demonstrated eight distinguishable current levels, but considering the signal-to-noise-ratio SNR of our setup, one could certainly achieve more levels, in particular if the leakage currents could be reduced, but this is beyond the scope of this paper.

We have already reported impressive retention times of the organic memory devices in our previous work [25]. We found that optically programmed states are very stable, and that the mild degradation observed for electrically programmed states may be resolved in the future by using more stable cathode materials.

The remaining challenge that needs to be addressed in future research efforts is the recording speed. While this can be increased in a straightforward manner for optical switching by using higher-intensity light sources, faster electrical recording would require similar DTE molecules that can provide higher quantum yields for the current-induced ring-closure reaction. While these photochromic light-emitting diodes may not represent the future of non-volatile storage media, they may find niche applications, e.g. RFID devices and gray scale signage [19].

#### Acknowledgement

We thank Merck KGaA (Darmstadt, Germany) for providing the blue-emissive polymer. We acknowledge funding by the State of Northrhine-Westfalia and the Europäische Fonds für Regionale Entwicklung (EFRE) through the PROTECT project, which is part of the Centre of Organic Production Technologies COPT.NRW.

#### Appendix A. Supplementary material

Supplementary data associated with this article can be found, in the online version, at <http://dx.doi.org/10.1016/j.orgel.2014.10.011>.

#### References

- [1] L. Ma, J. Liu, S. Pyo, Y. Yang, Organic bistable light-emitting devices, *Appl. Phys. Lett.* 80 (2002) 362–364.
- [2] J. Ouyang, C.-W. Chu, C.R. Szmanda, L. Ma, Y. Yang, Programmable polymer thin film and non-volatile memory device, *Nat. Mater.* 3 (2004) 918–922.
- [3] P. Heremans, G.H. Gelinck, R. Müller, K.-J. Baeg, D.-Y. Kim, Y.-Y. Noh, Polymer and organic nonvolatile memory devices †, *Chem. Mater.* 23 (2011) 341–358.
- [4] K. Asadi, P.W.M. Blom, D.M. de Leeuw, The MEMOLED: active addressing with passive driving, *Adv. Mater.* 23 (2011) 865–868.
- [5] M.H. Kryder, After hard drives—what comes next?, *IEEE Trans Magn.* 45 (2009) 3406–3413.
- [6] B.C. Das, A.J. Pal, Switching between different conformers of a molecule: multilevel memory elements, *Org. Electron.* 9 (2008) 39–44.
- [7] J.-G. Park, W.-S. Nam, S.-H. Seo, Y.-G. Kim, Y.-H. Oh, G.-S. Lee, et al., Multilevel nonvolatile small-molecule memory cell embedded with Ni nanocrystals surrounded by a NiO tunneling barrier, *Nano Lett.* 9 (2009) 1713–1719.
- [8] M. Lauters, B. McCarthy, D. Sarid, G.E. Jabbour, Multilevel conductance switching in polymer films, *Appl. Phys. Lett.* 89 (2006) 013507.
- [9] C. Wu, F. Li, Y. Zhang, T. Guo, T. Chen, Highly reproducible memory effect of organic multilevel resistive-switch device utilizing graphene oxide sheets/polyimide hybrid nanocomposite, *Appl. Phys. Lett.* 99 (2011) 042108.
- [10] L. Pellegrino, N. Manca, T. Kanki, H. Tanaka, M. Biasotti, E. Bellingeri, et al., Multistate memory devices based on free-standing VO(2)/TiO(2) microstructures driven by Joule self-heating, *Adv. Mater.* 24 (2012) 2929–2934.
- [11] B. Hu, X. Zhu, X. Chen, L. Pan, S. Peng, Y. Wu, et al., A multilevel memory based on proton-doped polyazomethine with an excellent uniformity in resistive switching, *J. Am. Chem. Soc.* 134 (2012) 17408–17411.
- [12] S.K. Hwang, J.M. Lee, S. Kim, J.S. Park, H. Il Park, C.W. Ahn, et al., Flexible multilevel resistive memory with controlled charge trap B- and N-doped carbon nanotubes, *Nano Lett.* 12 (2012) 2217–2221.
- [13] K. Asadi, M. Li, N. Stingelin, P.W.M. Blom, D.M. de Leeuw, Crossbar memory array of organic bistable rectifying diodes for nonvolatile data storage, *Appl. Phys. Lett.* 97 (2010) 193308.
- [14] A.J.J.M. van Breemen, J.-L. van der Steen, G. van Heck, R. Wang, V. Khikhlovskiy, M. Kemerink, et al., Crossbar arrays of nonvolatile, rewritable polymer ferroelectric diode memories on plastic substrates, *Appl. Phys. Exp.* 7 (2014) 031602.
- [15] J.C. Scott, Materials science. Is there an immortal memory?, *Science* 304 (2004) 62–63.
- [16] T.-W. Kim, D.F. Zeigler, O. Acton, H.-L. Yip, H. Ma, A.K.-Y. Jen, All-organic photopatterned one diode-one resistor cell array for advanced organic nonvolatile memory applications, *Adv. Mater.* 24 (2012) 828–833.
- [17] G.H. Kim, J.H. Lee, Y. Ahn, W. Jeon, S.J. Song, J.Y. Seok, et al., 32 × 32 Crossbar array resistive memory composed of a stacked schottky diode and unipolar resistive memory, *Adv. Funct. Mater.* 23 (2012) 1440–1449.
- [18] P. Zacharias, M.C. Gather, A. Köhnen, N. Rehm, K. Meerholz, Photoprogrammable organic light-emitting diodes, *Angew. Chem. Int. Ed. Engl.* 48 (2009) 4038–4041.
- [19] R.C. Shallock, P. Zacharias, A. Köhnen, P.O. Körner, E. Maibach, K. Meerholz, Photochromic transduction layers in organic memory elements, *Adv. Mater.* 25 (2013) 469–476.
- [20] M. Irie, Diarylethenes for memories and switches, *Chem. Rev.* 100 (2000) 1685–1716.
- [21] T. Tsujioka, H. Kondo, Organic bistable molecular memory using photochromic diarylethene, *Appl. Phys. Lett.* 83 (2003) 937–939.
- [22] E. Orgiu, N. Crivillers, M. Herder, L. Grubert, M. Pätzel, J. Frisch, et al., Optically switchable transistor via energy-level phototuning in a bicomponent organic semiconductor, *Nat. Chem.* 4 (2012) 675–679.
- [23] W.R. Browne, J.J.D. de Jong, T. Kudernac, M. Walko, L.N. Lucas, K. Uchida, et al., Oxidative electrochemical switching in dithienylcyclopentenes, part 1: effect of electronic perturbation on the efficiency and direction of molecular switching, *Chem. Eur. J.* 11 (2005) 6414–6429.
- [24] T. Tsujioka, T. Sasa, Y. Kakihara, Nonvolatile organic memory based on isomerization of diarylethene molecules by electrical carrier injection, *Org. Electron.* 13 (2012) 681–686.
- [25] R.C. Shallock, P.O. Körner, E. Maibach, A. Köhnen, K. Meerholz, A photochromic diode with a continuum of intermediate states: towards high density multilevel storage, *Adv. Mater.* 25 (2013) 4807–4813.